doi: 10.82124/CEAS-GNC-2026-093 CEAS-GNC-2026-093

EuroGNC Navigation Guidance Control CEAS Madrid, Spain May 5th-7th uc3m Universidad Carlos III de Madrid AIAA 2026

Modeling and attitude control of a flexible spacecraft with a rotating antenna

Daniel Alazard Professor, Fédération ENAC ISAE-SUPAERO ONERA, Université de Toulouse, Toulouse, France. daniel.alazard@isae-supaero.fr

Francesco Sanfedino Associate Professor, Fédération ENAC ISAE-SUPAERO ONERA, Université de Toulouse, Toulouse, France. francesco.sanfedino@isae-supaero.fr

Andre Marrazza Research engineer, DYCSYT, Toulouse, France. andrea.marrazza@dycsyt.com

Ervan Kassarian Robust control expert, DYCSYT, Toulouse, France. ervan.kassarian@dycsyt.com

ABSTRACT

The three-axis model of spacecraft fitted with flexible solar panels and a rotating RF (Radio-Frequency) antenna is derived. This model is fully parametrized according to the uncertain dynamic parameters (mass, centering, inertia, flexible mode frequencies) and varying parameters (solar array angular configuration, RF antenna rotating rate). A robust three-axis attitude controller is then designed to reject orbital disturbances. A pointing error budget is then performed to assess the effects of the disturbances coming from the Solar Array Driving Mechanism (SADM) and the time-periodic disturbance coming from the rotating RF antenna.

Keywords: Flexible structures, robust control, spacecraft, gyroscopic mode, Linear Time Periodic, Linear Parameter Varying.

Nomenclature

A calligraphic letter (for example, $\mathscr{B}$) is used to label a rigid body. The same uppercase letter (B) is used to denote its center of mass (CoM). The subscript with the same lower case letter (b) is used to denote its body frame and reference axes (for example, $\mathscr{R}_b = (O, \mathbf{x}_b, \mathbf{y}_b, \mathbf{z}_b)$ is the body frame attached to $\mathscr{B}$ at the reference point O). Additionally, the following notations will be used throughout this paper:

$m^{\mathscr{B}}$	mass of body $\mathscr{B}$ (kg).
$\mathbf{I}_P^{\mathscr{B}}$	3×3 inertia tensor of body $\mathscr{B}$ at point P $(kg\,m^2)$.
$\overrightarrow{PC}$	The vector from point P to point C (3×1 vector, m).
$\mathbf{P}_{a/b}$	3×3 Direction Cosine Matrix (DCM) of the rotation from frame $\mathscr{R}_a$ to frame $\mathscr{R}_b$, that contains the coordinates of vectors $\mathbf{x}_a$, $\mathbf{y}_a$, $\mathbf{z}_a$ expressed in frame $\mathscr{R}_b$.
$\omega_j^{\mathscr{B}}$	j-th flexible mode frequency of body $\mathscr{B}$ (rad/s).
$\left[\mathbf{L}_O^{\mathscr{B}}\right]_{\mathscr{R}_b}$	Matrix of modal participation factors of the flexible modes of the body $\mathscr{B}$ at the point O and projected in the frame $\mathscr{R}_b$ ($n \times 6$ matrix for n flexible modes, $\sqrt{kg}$, $\sqrt{kg}\,m$).
$\mathbf{R}_{\mathbf{v}}(\alpha)$	DCM associated to the rotation of α (rad) around the vector $\mathbf{v}$.
$\boldsymbol{\omega}^{\mathscr{B}}$	Angular speed of $\mathscr{R}_b$ with respect to inertial frame $\mathscr{R}_i$ (3×1 vector, rad/s).
$\mathbf{a}_P^{\mathscr{B}}$	Inertial acceleration of body $\mathscr{B}$ at point P (3×1 vector, m/s^2).

$\mathbf{F}_{\mathscr{B}/\mathscr{A}}$	Force applied by body $\mathscr{B}$ on body $\mathscr{A}$ (3×1 vector, N).
$\mathbf{T}_{\mathscr{B}/\mathscr{A},P}$	Torque applied by $\mathscr{B}$ on $\mathscr{A}$ at point P (3×1 vector, Nm).
$[\star]_{\mathscr{R}_b}$	Projection of $\star$ (vector, wrench, tensor, model,...) in the frame $\mathscr{R}_b$. For a vector $\mathbf{v}$: $[\mathbf{v}]_{\mathscr{R}_b} = \mathbf{P}_{a/b}[\mathbf{v}]_{\mathscr{R}_a}$.
$\mathbf{W}_{\mathscr{B}/\mathscr{A},P}$	6×1 wrench applied by $\mathscr{B}$ on $\mathscr{A}$ at point P: $\mathbf{W}_{\mathscr{B}/\mathscr{A},P} = \begin{bmatrix} \mathbf{F}_{\mathscr{B}/\mathscr{A}} \\ \mathbf{T}_{\mathscr{B}/\mathscr{A},P} \end{bmatrix}$.
$\mathbf{W}_{./\mathscr{A},P}$	6×1 local wrench applied on $\mathscr{A}$ at point P.
$\mathbf{W}_{\mathscr{A}/.,P}$	6×1 local wrench applied by $\mathscr{A}$ at point P.
$\frac{d\mathbf{v}}{dt}\big\vert_{\mathscr{R}}$	Time-derivative w.r.t. frame $\mathscr{R}$ of the vector $\mathbf{v}$ $\left(\left[\frac{d\mathbf{v}}{dt}\vert_{\mathscr{R}}\right]_{\mathscr{R}} = \frac{d[\mathbf{v}]_{\mathscr{R}}}{dt}\right)$.
$\dot{\mathbf{v}}^{\mathscr{B}}$	Time-derivative of the vector $\dot{\mathbf{v}}^{\mathscr{B}}$ in the body frame: $\dot{\mathbf{v}}^{\mathscr{B}} = \frac{d\mathbf{v}^{\mathscr{B}}}{dt}\vert_{\mathscr{R}_b}$
$\ddot{\mathbf{u}}_P^{\mathscr{B}}$	6×1 acceleration dual vector of body $\mathscr{B}$ at point P: $\ddot{\mathbf{u}}_P^{\mathscr{B}} = \begin{bmatrix} \mathbf{a}_P^{\mathscr{B}} \\ \dot{\boldsymbol{\omega}}^{\mathscr{B}} \end{bmatrix}$.
$\mathbf{P}_{a/b}^{\times 2}$	Augmented DCM for dual vectors $\mathbf{P}_{a/b}^{\times 2} = \text{diag}\left(\mathbf{P}_{a/b}, \mathbf{P}_{a/b}\right)$.
$\mathbf{D}_P^{\mathscr{A}}(\text{s})$	6×6 dynamic model of body $\mathscr{A}$ expressed at point P.
$\mathbf{D}_{PC}^{\mathscr{A}}(\text{s})$	12×12 TITOP dynamic model of body $\mathscr{A}$ expressed at points P and C.
$({}^*\mathbf{x})$	Skew-symmetric matrix associated to the 3×1 vector $\mathbf{x}$: $({}^*\mathbf{x}) = \begin{bmatrix} 0 & -\mathbf{x}(3) & \mathbf{x}(2) \\ \mathbf{x}(3) & 0 & -\mathbf{x}(1) \\ -\mathbf{x}(2) & \mathbf{x}(1) & 0 \end{bmatrix}$
s	Laplace's variable.
$\mathbf{1}_n$	Identity matrix $n \times n$.
$\mathbf{0}_{n \times m}$	Zero matrix $n \times m$.
$\mathbf{A}^T$	Transpose of $\mathbf{A}$.
diag	Diagonal augmentation.
$\mathbf{G}_{(i:j,k:l)}(\text{s})$	Sub-system of $\mathbf{G}(\text{s})$ restricted to outputs i to j and the inputs k to l.

1 Introduction

The space missions become more and more challenging, which is pushing the industry and agencies towards the development of advanced solutions at different system levels: payload, satellite platform, and data processing. Higher-quality products for Earth observation (EO) and science require satisfying stringent pointing requirements in terms of both accuracy and stability [1]. One of the most significant sources of the pointing errors is the internal disturbances due to the on-board mechanisms such as actuator vibrations (e.g., RWS, SADM, etc.), transient and vibrations induced by flexible modes excitation (e.g., solar arrays), payload motion (e.g., in RF instruments), sloshing, etc.

In addition, space engineering requires modeling, control and analysis tools allowing to assess the robustness of the pointing performances in spite of the uncertainties on the mechanical parameters or the variations on the geometric or kinematic configurations. These tools should allow us to eliminate faulty designs as early as possible during the preliminary phase to avoid very time-consuming iterations between mechanical design, control design, validation and verification. The SDTlib [2, 3] is a modeling tool developed in that spirit. It allows us to derive the LTI (Linear Time-Invariant) model of a flexible multi-body system, fully parameterized with respect to the varying or uncertain parameters. Such a model can then directly be used with the Matlab Robust Control Toolbox for robust control design or robustness analysis.

The SDTlib is based on the TITOP (Two-Input Two-Output Ports) modeling approach [4] which allows the system overall model to be assembled from the models of the mechanical/structural sub-components. It was successfully used in [5] to analyze the vibrations induced by the SADM on an Earth-observation satellite: the diverging then converging pointing oscillations observed in the telemetry data over one orbital period can therefore be explained by the varying dynamic coupling between the main body and the solar array, depending on its angular configuration. In [6] the SDTlib was used to evaluate the active and/or passive solutions in order to isolate the line of sight of a telescope from the internal disturbances coming from the spacecraft. Static and dynamic unbalances in rotating device are one of the most significant sources of internal disturbances. They are studied in [7] for reaction wheels mounted on an active and/or passive isolator. A larger rotating device like an RF antenna is accurately modeled in [8] using KANE's equations and a finite-element model. In this article, the rotating RF antenna is modeled using the TITOP formalism to obtain a model valid for any antenna angular velocity and to assess the parametric robustness of the pointing performance of the satellite carrying the antenna.

The basics of TITOP models are first reminded in section 2. Section 3 is devoted to the LTP (Linear-Time-Periodic) model of a rotating RF antenna linked to the spacecraft main body through a flexible boom. This model, linearized around a given (but varying) angular rate, is developed to be fully compliant with the TITOP approach. It can thus be assembled to the whole model while taking into account all gyroscopic couplings and the time-periodic disturbance due to the dynamic unbalances in the RF antenna. In section 4, the model of a spacecraft including flexible solar panels (with a varying angular configuration $\theta \in [-\pi,\ \pi]$), a rotating RF antenna (at the varying angular rate Ω) linked to the main body by a flexible boom and a compensation wheel is then derived using the SDTlib. Then a robust structured 3-axis attitude controller is designed on the LTI model (assuming $\Omega = 0$) to:

- reject orbital disturbances and meet a requirement on the Absolute Pointing Error (APE),
- meet stability margin requirements,
- while minimizing the APE in response to the harmonic disturbance due to the rotating antenna unbalances.

The worst-case pointing error due to the internal disturbances (SADM disturbing torque and time-periodic excitation due to the RF antenna unbalances) is addressed in section 5 considering Ω as a varying parameter. The FLOQUET theory [9] is then used to assess the stability of the LTP model evaluated on the worst-case parametric configuration.

2 Basics on TITOP modelling approach

Let us consider a flexible body $\mathscr{A}$ as seen in Fig. 1 (left) connected to a parent structure $\mathscr{P}$ at the point P and to a child structure $\mathscr{C}$ at the point C. The resulting TITOP model $\mathbf{D}^{\mathscr{A}}_{PC}(\mathrm{s})$, schematized in Fig. 1 (right), is a 12×12 linear dynamic model whose inputs are:

- $\mathbf{W}_{\mathscr{C}/\mathscr{A},C}$: the 6×1 wrench (forces and torques) applied by the body $\mathscr{C}$ to $\mathscr{A}$ at point C;
- $\ddot{\mathbf{u}}^{\mathscr{A}}_{P}$: the 6×1 dual vector of inertial accelerations (linear and angular) imposed by the parent body $\mathscr{P}$ at point P to $\mathscr{A}$;

and the conjugated outputs are:

- $\ddot{\mathbf{u}}_{C}$: the 6×1 dual vector of inertial accelerations (linear and angular) of point C;
- $\mathbf{W}_{\mathscr{A}/\mathscr{P},P}$: the 6×1 wrench applied by $\mathscr{A}$ to the parent structure $\mathscr{P}$ at point P.

All these input/output variables are projected in the body frame $\mathscr{R}_a$.

As described in [4], the state-space representation of $\mathbf{D}^{\mathscr{A}}_{PC}(\mathrm{s})$ can be built directly from the mechanical parameters of the body $\mathscr{A}$ (expressed in $\mathscr{R}_a$ for vectors and tensors):

- $m^{\mathscr{A}}$, $\mathbf{I}^{\mathscr{A}}_{G}$: mass and 3×3 inertia tensor at the CoM G (center of Mass) of body $\mathscr{A}$,

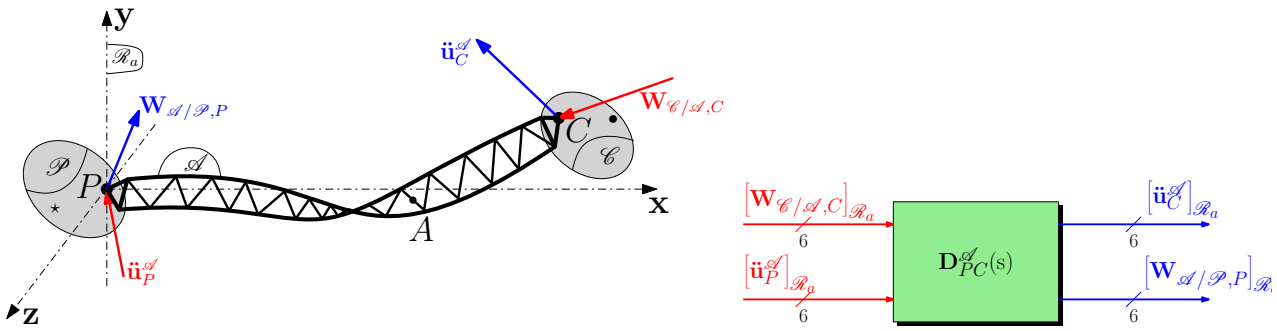

Fig. 1 TITOP scheme and nomenclature for a generic flexible appendage $\mathscr{A}$.

- $\overrightarrow{PA}$, $\overrightarrow{PC}$: the geometry of the body $\mathscr{A}$,
- the frequencies, the modal participation factors at the point P, the projections at the point C of the various flexible modes taken into account [4]. In SDTlib, these data can be read from the NASTRAN output files of the body $\mathscr{A}$ when clamped at P and free at C (through a NASTRAN/SIMULINK interface) or derived analytically for a simple-shaped body (beams and plates) .

Then the model of the assembly of this body $\mathscr{A}$, the parent body $\mathscr{P}$ (itself connected at the point $\star$ to another body) and the child body $\mathscr{C}$ (itself connected at the point $\bullet$ to another body) is performed by the feedback inter-connections of the TITOP models of the various elements through the DCMs (Direct Cosine Matrices) between the body frames, as depicted in Figure 2.

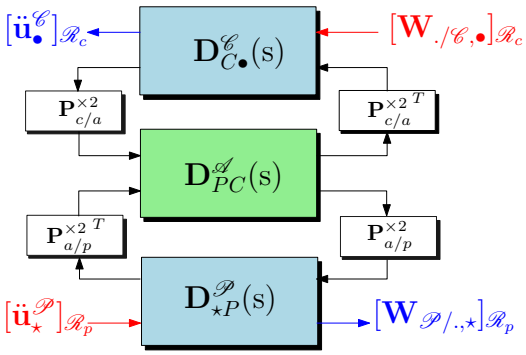

Fig. 2 Model of the assembly of the body $\mathscr{A}$ between bodies $\mathscr{P}$ and $\mathscr{C}$ using TITOP models.

When the bodies $\mathscr{P}$ and $\mathscr{A}$ are connected at the point P through a revolute joint with a time-varying configuration θ, the DCM $\mathbf{P}_{a/p}(\theta)$, which now depends on θ, can be expressed as an LFT (Linear Fractionar Transformation) involving the new parameterization $\sigma = \tan(\theta/4)$ (see also: [10]) and thus be included in the LPV (Linear Parameter Varying) model of the system (σ is then considered as a vaying parameter; not as a state variable). Finally the TITOP model of the revolute joint includes also an additionnal SISO (Single-Input Single-Output) channel between the torque applied inside the revolute joint by a local actuator (for instance the SADM as it will be the case in section 4) and the in-joint angular acceleration $\ddot{\theta}$ (assumed to be small to satisfy the linearity assumption). This channel can be used to take into account a model of the local mechanism (see section 4).

3 LTP model of a rotating antenna

Consider the rotating RF antenna (appenda $\mathscr{A}$ in red in Figure 3) connected at the point P to a cantilevered boom on the main body $\mathscr{B}$. This antenna is driven at a constant angular rate Ω around a direction $\mathbf{v}$. Note that in the general case the center of mass G of the appendage $\mathscr{A}$ may not be coincident

with the connecting point P and that the reflector can also be tilted with an angle α w.r.t. to the plane orthogonal to the spin axis $\mathbf{v}$. So disturbances due to the static and dynamic unbalances must be taken into account.

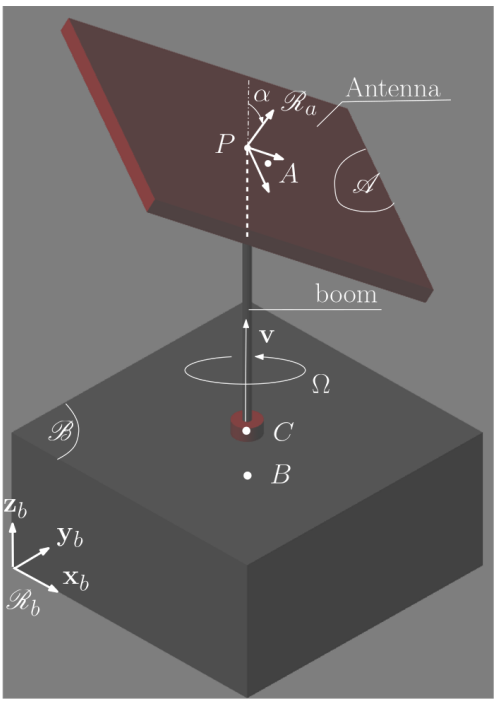

Fig. 3 A rigid rotating antenna on a rigid spacecraft.

The objective is to derive an LTP model capturing all the couplings between the various subsystems and modeling the internal disturbances due to unbalances which can be fully parametrized according to the spin rate Ω with LFT formalism. Such a model can then be used like any other blocks in the SDTlib. Thanks to the Euler-Newton equations [11], the direct dynamic model between the interaction wrench $\mathbf{W}_{\mathscr{B}/\mathscr{A},P} = \begin{bmatrix} \mathbf{F}_{\mathscr{B}/\mathscr{A}} \\ \mathbf{T}_{\mathscr{B}/\mathscr{A},P} \end{bmatrix}$ and the dual acceleration vector $\ddot{\mathbf{u}}_P^{\mathscr{A}} = \begin{bmatrix} \mathbf{a}_P^{\mathscr{A}} \\ \dot{\boldsymbol{\omega}}^{\mathscr{A}} \end{bmatrix}$ at the point P of the appendage $\mathscr{A}$ reads:

$$\begin{bmatrix} \mathbf{F}_{\mathscr{B}/\mathscr{A}} \\ \mathbf{T}_{\mathscr{B}/\mathscr{A},P} \end{bmatrix} = \underbrace{\begin{bmatrix} m^{\mathscr{A}}\mathbf{1}_3 & m^{\mathscr{A}}\,(^*\overrightarrow{AP}) \\ -m^{\mathscr{A}}\,(^*\overrightarrow{AP}) & \underbrace{\mathbf{I}_A^{\mathscr{A}} - m^{\mathscr{A}}\,(^*\overrightarrow{AP})^2}_{\mathbf{I}_P^{\mathscr{A}}} \end{bmatrix}}_{\mathbf{D}_P^{\mathscr{A}}} \begin{bmatrix} \mathbf{a}_P^{\mathscr{A}} \\ \dot{\boldsymbol{\omega}}^{\mathscr{A}} \end{bmatrix} + \begin{bmatrix} -m^{\mathscr{A}}\,(^*\boldsymbol{\omega}^{\mathscr{A}})^2\overrightarrow{GP} \\ (^*\boldsymbol{\omega}^{\mathscr{A}})\mathbf{I}_P^{\mathscr{A}}\boldsymbol{\omega}^{\mathscr{A}} \end{bmatrix} \tag{1}$$

where $(^*\mathbf{x})$ is the skew-symmetric matrix associated to the vector $\mathbf{x}$.

This equation is valid in any frame but will be projected in the frame $\mathscr{R}_a$ attached to the rotating appendage $\mathscr{A}$ where $\mathbf{D}_P^{\mathscr{A}}$ is constant. Considering that the appendage $\mathscr{A}$ is rotating w.r.t. body $\mathscr{B}$ with an angular rate Ω around $\mathbf{v}$, one can write:

$$\mathbf{a}_p^{\mathscr{A}} = \mathbf{a}_P^{\mathscr{B}}$$

$$\boldsymbol{\omega}^{\mathscr{A}} = \boldsymbol{\omega}^{\mathscr{B}} + \Omega\mathbf{v}$$

$$\text{and } \left[\dot{\boldsymbol{\omega}}^{\mathscr{A}}\right]_{\mathscr{R}_a} = \left[\left.\frac{d\boldsymbol{\omega}^{\mathscr{A}}}{dt}\right|_{\mathscr{R}_a}\right]_{\mathscr{R}_a} = \left[\left.\frac{d\boldsymbol{\omega}^{\mathscr{B}}}{dt}\right|_{\mathscr{R}_a} + \mathbf{0}\right]_{\mathscr{R}_a} = \left[\left.\frac{d\boldsymbol{\omega}^{\mathscr{B}}}{dt}\right|_{\mathscr{R}_b} - \Omega(^*\mathbf{v})\boldsymbol{\omega}^{\mathscr{B}}\right]_{\mathscr{R}_a} = \left[\dot{\boldsymbol{\omega}}^{\mathscr{B}} - \Omega(^*\mathbf{v})\boldsymbol{\omega}^{\mathscr{B}}\right]_{\mathscr{R}_a}.$$

Assuming that $\boldsymbol{\omega}^{\mathscr{B}}$ and $\dot{\boldsymbol{\omega}}^{\mathscr{B}}$ are small, one can perform a first order expansion of the Newton-Euler equation. After some algebra (and the use of Jacobi identity to factorize $\boldsymbol{\omega}^{\mathscr{B}}$ on the right in the right-hand term of equation (1):

$({}^*\boldsymbol{\omega}^{\mathscr{B}})({}^*\mathbf{v})\overrightarrow{AP} = ({}^*\overrightarrow{AP})({}^*\mathbf{v})\boldsymbol{\omega}^{\mathscr{B}} - ({}^*\mathbf{v})({}^*\overrightarrow{AP})\boldsymbol{\omega}^{\mathscr{B}}$ and $({}^*\mathbf{v})({}^*\boldsymbol{\omega}^{\mathscr{B}})\overrightarrow{AP} = -({}^*\mathbf{v})({}^*\overrightarrow{AP})\boldsymbol{\omega}^{\mathscr{B}}$.

This first-order model reads:

$$\left[\begin{array}{c}\mathbf{F}_{\mathscr{B}/\mathscr{A}}\\ \mathbf{T}_{\mathscr{B}/\mathscr{A},P}\end{array}\right]_{\mathscr{R}_a} = \left[\mathbf{D}_P^{\mathscr{A}}\left[\begin{array}{c}\mathbf{a}_P^{\mathscr{B}}\\ \boldsymbol{\omega}^{\mathscr{B}}\end{array}\right] + \underbrace{\Omega^2\left[\begin{array}{c}-m^{\mathscr{A}}({}^*\mathbf{v})^2\overrightarrow{AP}\\ ({}^*\mathbf{v})\mathbf{I}_P^{\mathscr{A}}\mathbf{v}\end{array}\right]}_{\overline{\mathbf{W}}_{pert}(\Omega)} + \underbrace{\Omega\left[\begin{array}{c}2m^{\mathscr{A}}\left[({}^*\mathbf{v})({}^*\overrightarrow{AP}) - ({}^*\overrightarrow{AP})({}^*\mathbf{v})\right]\\ \left[({}^*\mathbf{v})\mathbf{I}_P^{\mathscr{A}} - \mathbf{I}_P^{\mathscr{A}}({}^*\mathbf{v}) - ({}^*\mathbf{I}_P^{\mathscr{A}}\mathbf{v})\right]\end{array}\right]}_{\mathbf{G}_P^{\mathscr{A}}(\Omega)}\boldsymbol{\omega}^{\mathscr{B}}\right]_{\mathscr{R}_a} \quad (2)$$

$\overline{\mathbf{W}}_{pert}(\Omega)$ and $\mathbf{G}_P^{\mathscr{A}}(\Omega)$ are the inertial disturbing torque due to the unbalances in the appendage and the gyroscopic gain, respectively. They are constant in the frame $\mathscr{R}_a$ but periodic (with the period $2\pi/\Omega$) in the frame $\mathscr{R}_b$.

Let us denote: $\mathbf{P}_{a/b}(\Omega t) = \mathbf{R}_{\mathbf{v}}(\Omega t)\mathbf{R}_{\mathbf{v}^\perp}(\alpha)$ the time-periodic DCM (Direction Cosine Matrix) from frame $\mathscr{R}_a$ to frame $\mathscr{R}_b$ where $\mathbf{R}_{\mathbf{v}^\perp}(\alpha)$ is the DCM associated with the tilt angle about any axis orthogonal to the spin direction $\mathbf{v}$. Then the model of the appendage $\mathscr{A}$ must be connected to the associated port of the TITOP model of the body $\mathscr{B}$ which inputs and ouputs are $\left[\begin{array}{c}\mathbf{F}_{\mathscr{B}/\mathscr{A}}\\ \mathbf{T}_{\mathscr{B}/\mathscr{A},P}\end{array}\right]_{\mathscr{R}_b}$ and $\left[\begin{array}{c}\mathbf{a}_P^{\mathscr{B}}\\ \dot{\boldsymbol{\omega}}^{\mathscr{B}}\end{array}\right]_{\mathscr{R}_b}$ (i.e: interaction wrench and dual acceleration vector projected in the frame $\mathscr{R}_b$). Thus the first order model of the rotating appendage is an LTP (Linear Time Periodic) system with in addition a time-periodic perturbation and reads:

$$\begin{aligned}\left[\begin{array}{c}\mathbf{F}_{\mathscr{B}/\mathscr{A}}\\ \mathbf{T}_{\mathscr{B}/\mathscr{A},P}\end{array}\right]_{\mathscr{R}_b} &= \mathbf{P}_{b/a}^{\times 2}(\Omega t)\left(\left[\mathbf{D}_P^{\mathscr{A}}\right]_{\mathscr{R}_a}\mathbf{P}_{b/a}^{\times 2\,T}(\Omega t)\left[\begin{array}{c}\mathbf{a}_P^{\mathscr{B}}\\ \dot{\boldsymbol{\omega}}^{\mathscr{B}}\end{array}\right]_{\mathscr{R}_b} \cdots\right. \quad (3)\\ &\quad \left. + \left[\overline{\mathbf{W}}_{pert}(\Omega)\right]_{\mathscr{R}_a} + \left[\mathbf{G}_P^{\mathscr{A}}(\Omega)\right]_{\mathscr{R}_a}\mathbf{P}_{b/a}^{T}(\Omega t)[\boldsymbol{\omega}^{\mathscr{B}}]_{\mathscr{R}_b}\right)\\ &= \left[\mathbf{D}_P^{\mathscr{A}}(\Omega t)\right]_{\mathscr{R}_b}\left[\begin{array}{c}\mathbf{a}_P^{\mathscr{B}}\\ \dot{\boldsymbol{\omega}}^{\mathscr{B}}\end{array}\right]_{\mathscr{R}_b} + \left[\overline{\mathbf{W}}_{pert}(\Omega, \Omega t)\right]_{\mathscr{R}_b} + \left[\mathbf{G}_P^{\mathscr{A}}(\Omega, \Omega t)\right]_{\mathscr{R}_b}[\boldsymbol{\omega}^{\mathscr{B}}]_{\mathscr{R}_b} \quad (4)\end{aligned}$$

and can represented by the block diagram representation depicted in Figure 4).

The input ports # 2 and 3 are logical valued inputs to switch on the simulation of the disturbance and the time-periodic dependence of the model. Note that in the case of an balanced antenna: $\overrightarrow{AP} = \mathbf{0}$ and $\mathbf{I}_P^{\mathscr{A}} = \left[\begin{array}{ccc}I_r & 0 & 0\\ 0 & I_r & 0\\ 0 & 0 & I_w\end{array}\right]$ (if $\mathbf{v}$ is aligned with the $\mathbf{z}$-axis of the wheel) then $\overline{\mathbf{W}}_{pert} = \mathbf{0}$ and one can recognize the model on a reaction wheel as already present in the SDTlib.

Such a block can be directly included in the model $\mathbf{G}_{LTP}(\mathrm{s})$ of the assembly as depicted in Figure 5 (left) which also details the main body $\mathscr{B}$ and the boom.

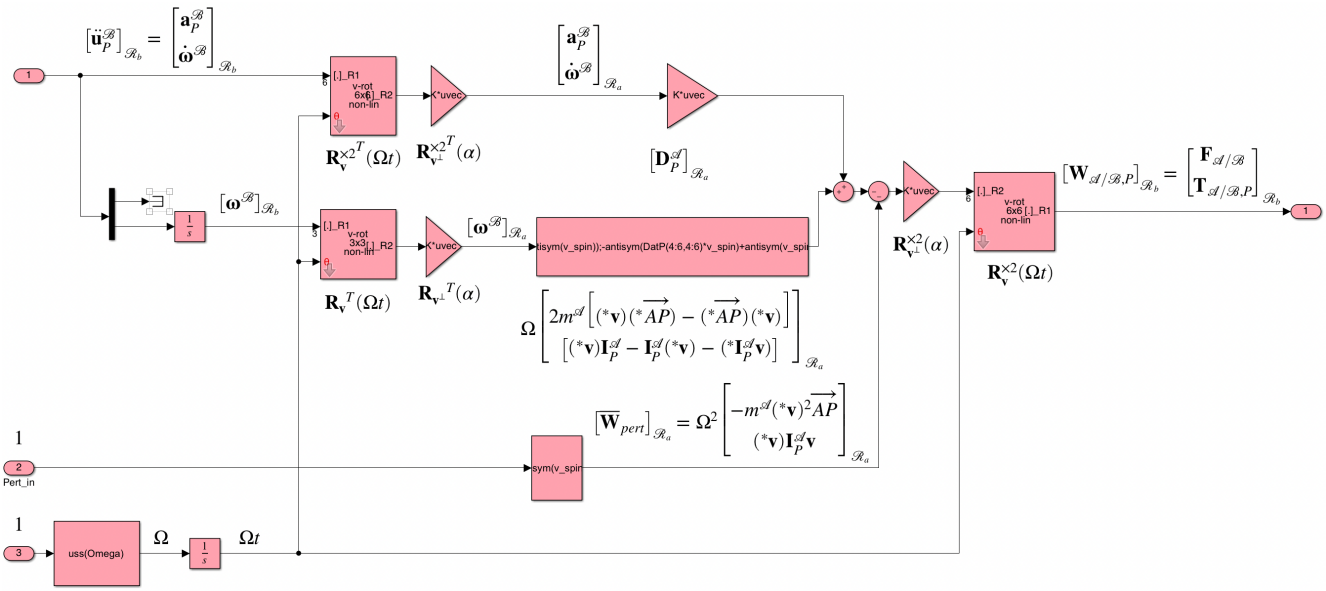

Fig. 4 LTP SDTlib model $\mathbf{D}_P^{\mathscr{A}}(\mathrm{s})$ of a rotating RF antenna.

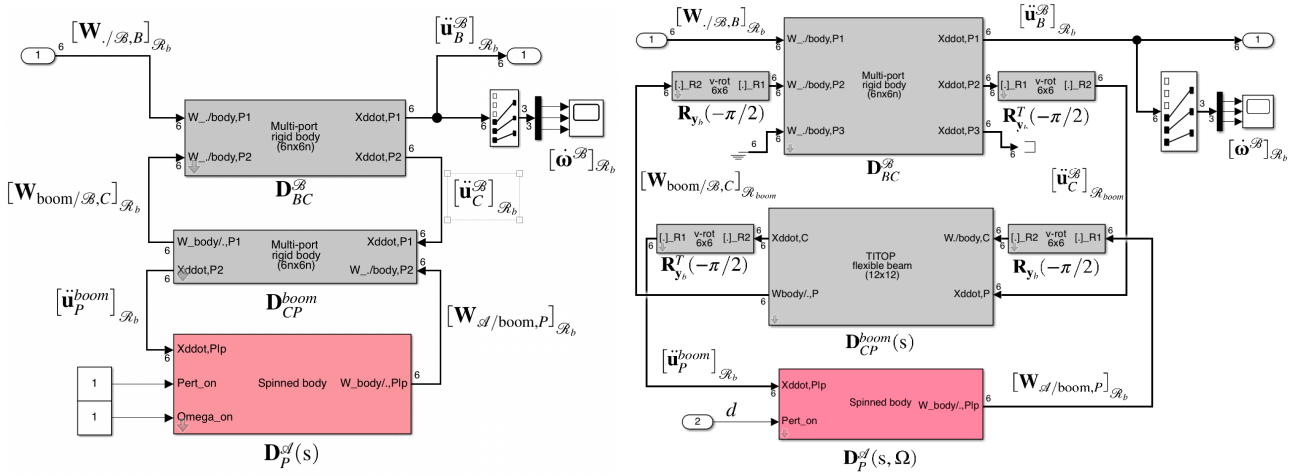

Fig. 5 Left: 6×6 LTP model $\mathbf{G}_{LTP}(\mathrm{s})$ of the main body $\mathscr{B}$ + rigid boom + RF antenna $\mathscr{A}$ - Right: 6×7 LPV model $\mathbf{G}_{LPV}(\mathrm{s})$ of the main body $\mathscr{B}$ + flexible boom + RF antenna $\mathscr{A}$ (note that DCMs are required to align the axis of the flexible beam with the spin axis.).

Numerical application: As an illustration, let us consider the case of an homogeneous main body $\mathscr{B}$ with a mass $m^{\mathscr{B}} = 1000\,kg$ and a cubic shape $2 \times 2 \times 1\,(m)$, a $1\,kg$ boom with a cross section of $25\,cm^2$, a length of $2\,m$ along $\mathbf{z}_b$ and an homogeneous reflector $\mathscr{A}$ with a mass $m^{\mathscr{A}} = 20\,kg$ and a cubic shape $2 \times 2 \times 0.1\,(m)$ rotating around $\mathbf{v} = \mathbf{z}_b$ at $\Omega = 15$ rpm and tilt with an angle $\alpha = 30\,deg$.

Then, the time-domain response of the angular acceleration $\left[\dot{\boldsymbol{\omega}}^{\mathscr{B}}\right]_{\mathscr{R}_b}$ (roll, pitch and yaw in rad/s^2) of the main body $\mathscr{B}$ due to the harmonic disturbance $\overline{\mathbf{W}}_{pert}(\Omega)$, obtained from the model $\mathbf{G}_{LTP}(\mathrm{s})$ (Figure 5-left), is depicted in Figure 6 (dash black line) and compared with the non-linear simulation made with Simscape/Multibody (solid green line). One can verify the perfect matching between the two models and, therefore, the validity of the linearity assumption. These responses illustrate also the impact on the main body of the dynamic unbalances in the rotating RF antenna (note that in this case there is no static unbalances since the center of mass G coincides with the connecting point P).

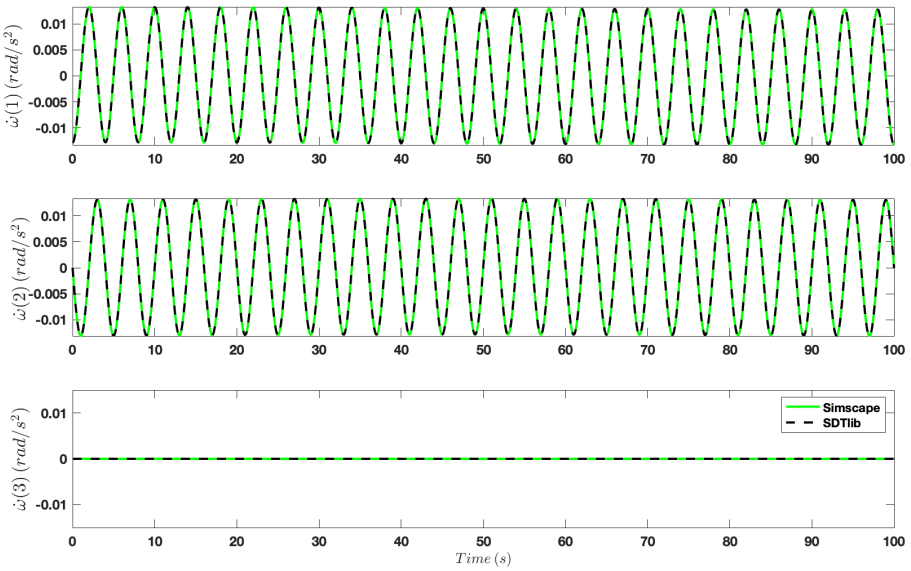

Fig. 6 Non-linear simulation performed thank to Simscape/Multibody (solid green) and comparison with the SDTlib linearized model (dash black).

For robust control design and pointing performance assessment, the previous LTP model can be turned into a parameterized LPV (Linear Parameter Varying) and LTI model considering:

- the uncertain parameter $\Omega t \in [-\pi,\ \pi]$ to represent a full revolution around the spin axis,
- the varying angular spin rate Ω involved in the gyroscopic gain $\mathbf{G}_P^{\mathscr{A}}(\Omega)$ and in the harmonic disturbance signal $\overline{\mathbf{W}}_{pert}(\Omega)$ which can be normalized thanks to the very selective unitary band-pass filter:

$$F_h(\mathrm{s}, \Omega) = \frac{0.0002\Omega\mathrm{s}}{\mathrm{s}^2 + 0.0002\Omega\mathrm{s} + \Omega^2} \tag{5}$$

  in order to capture the frequency domain response to this harmonic disturbance only at the spin rate Ω.

This LPV model is then detailed in the following Figure 7 and can be used in the model of the assembly depicted in Figure 5 (right) where the rigid boom was replaced by a flexible beam.

The harmonic exchange of the impact of the disturbance d on the $\mathbf{x}$ (roll) and the $\mathbf{y}$ (pitch) axes can be illustrated on the frequency-domain responses of the transfer from the disturbance input d to the angular accelerations evaluated when $\Omega t = 0$ and $\Omega t = \pi/2$ as depicted in Figure 8. These plots

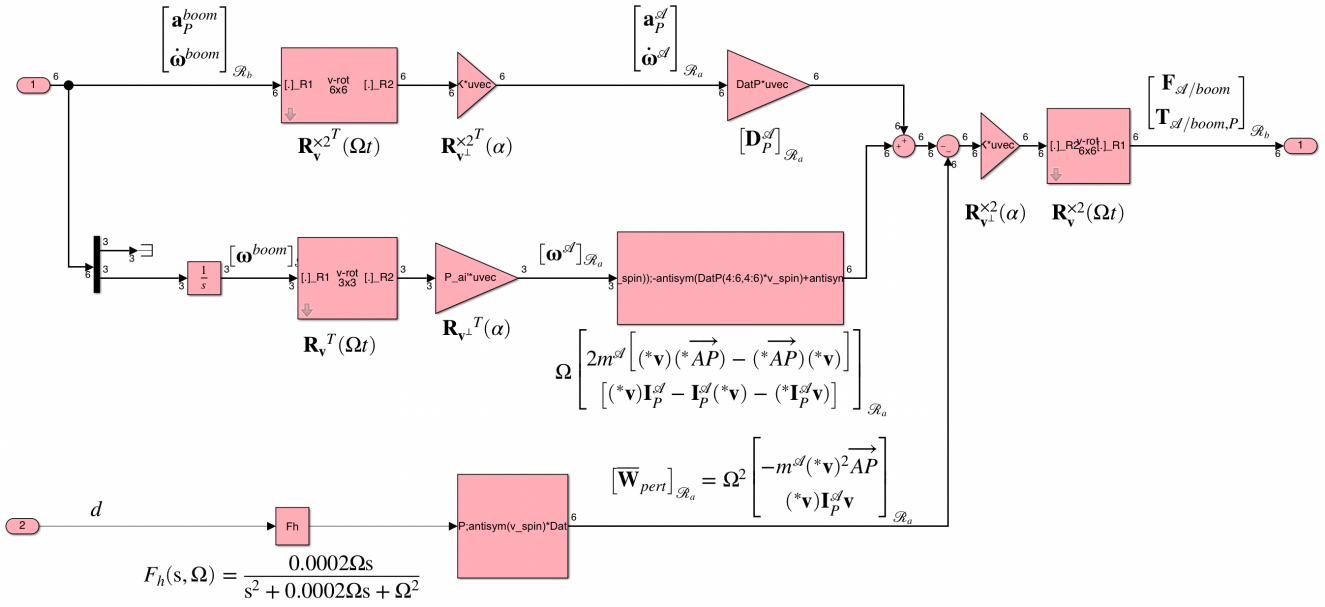

Fig. 7 LPV SDTlib model of a rotating RF antenna.

were obtained considering 20% of relative variation on the angular rate Ω (around the nominal value: 15 rpm $\approx 1.57\,rad/s$). One can also notice on these responses:

- the resonance around $0.03\,rad/s$ due to the gyroscopic mode. This mode will be compensated by a compensation wheel in the study case presented in section 4,
- the resonance at Ω due to the harmonic disturbance,
- the high-frequency resonances of the flexible modes of the beam.

The magnitude of the oscillations seen on the response of the Figure 6 in the nominal parametric configuration can then be evaluated by the magnitude of the transfer between the disturbance d (dimensionless) and the first component of the angular acceleration vector $\left[\dot{\boldsymbol{\omega}}^{\mathscr{B}}\right]_{\mathscr{R}_b}$:

$$|\mathbf{G}_{LPV_{(4,7)}}(\mathrm{j}\Omega)| = 0.013\ (rad/s^2)\ .$$

4 LTI robust control of a flexible spacecraft

4.1 Model

The considered study case is depicted in Figure 9. It is composed of:

- a rigid main body $\mathscr{B}$,
- two symmetrical solar arrays $\mathscr{A}_1$ and $\mathscr{A}_2$ at a varying angular configuration $\theta \in [-\pi,\ \pi]$,
- a rotating RF antenna $\mathscr{A}_3$ at the varying angular rate Ω linked to the main body by a flexible boom,
- a compensation wheel $\mathscr{A}_4$ (to cancel the angular momentum stored in the RF-antenna). This compensation wheel is spun at -10Ω and its main axis inertia is a tenth of the RF antenna inertia along the $\mathbf{y}_b$ axis.

In addition, to maintain the angular configuration of $\mathscr{A}_i$ $(i = 1, 2)$ w.r.t. $\mathscr{B}$ at the value θ, the SADM in the revolute joint at point P_i is modeled as a local stiffness k_i (Nm/rad), a viscous friction f_i (Nms/rad) and an internal disturbing torque p_i (Nm): $u_i = -k_i\delta\theta_i - f_i\dot{\delta\theta}_i + p_i$.

All the data and their uncertainties are defined in Table 2 in appendix.

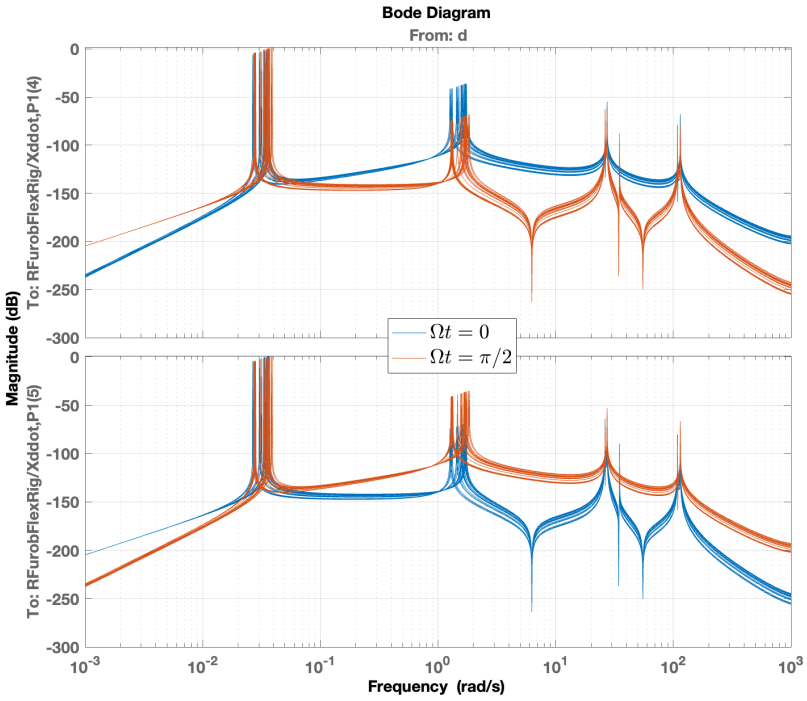

Fig. 8 Frequency domain responses of the transfer from the disturbance d to the roll angular acceleration (top: $\mathbf{G}_{LPV_{(4,7)}}(\mathrm{s})$) and pitch angular acceleration (bottom: $\mathbf{G}_{LPV_{(5,7)}}(\mathrm{s})$) for 2 angular configurations of the antenna ($\Omega t = 0,\ \pi/2$).

The 3×6 mechanical model $\mathbf{M}(\mathrm{s}, \mathbf{\Delta}, \theta, \Omega, \Omega t)$ of this spacecraft, built with the SDTlib, is then displayed in Figure 10. The 6 inputs are $\mathbf{u}\ (Nm)$, i.e. the external torque (3 components) applied on the spacecraft by the orbital disturbances and the attitude control system (ACS, not detailed in this paper), the 2 internal disturbances $p_1\ (Nm)$ and $p_2\ (Nm)$ due to the SDAMs and the disturbance d due to the unbalances of the rotating RF antenna. The 3 outputs are the 3 components of the main body angular rate $\left[\boldsymbol{\omega}^{\mathscr{B}}\right]_{\mathscr{R}_b}$. This model depends on:

- a vector of 7 uncertain parameters $\mathbf{\Delta} = [m^{\mathscr{B}},\ \mathrm{diag}\left(\left[\mathbf{I}_B^{\mathscr{B}}\right]_{\mathscr{R}_b}\right),\ \omega_j^{\mathscr{A}_1}]^T,\ j = 1, 2, 3$. It is assumed that the solar arrays are identical: $\omega_j^{\mathscr{A}_2} = \omega_j^{\mathscr{A}_1}, \forall j$,
- $\theta \in [-\pi,\ \pi]$ the angular configuration of the solar arrays,
- $\Omega t \in [-\pi,\ \pi]$ the angular configuration of the RF antenna,
- Ω the angular rate of the RF antenna involved in the gyroscopic gain $\left[\mathbf{G}_{A_3}^{\mathscr{A}_3}(\Omega, \Omega t)\right]_{\mathscr{R}_b}$ and the harmonic disturbance $\left[\overline{\mathbf{W}}_{pert}(\Omega, \Omega t)\right]_{\mathscr{R}_b}$ in (4). Note that in the LPV and LTI model Ω and Ωt are considered as two independent parameters.

Considering the nominal values for all the parameters $\mathbf{\Delta}$, θ and Ω, the Figure 11 plots the evolution with Ωt of the system dynamics. It is clear that the LTI (Linear Time Invariant) model obtained in some antenna angular configuration, for instance $\Omega t = \pi/4$, is unstable. This unstability is linked to the non positivity of the gyroscopic gain $\left[\mathbf{G}_{A_3}^{\mathscr{A}_3}(\Omega, \Omega t)\right]_{\mathscr{R}_b}$ in some configurations Ωt. It impacts the stability of 2 flexible modes around $29\,rad/s$ and $34\,rad/s$ which are too fast to be controlled by the ACS. Note also that such an LTI stability analysis is very penalizing since the time-periodic nature of the system is not considered. That is why we will assume that $\Omega = 0$ for the control design presented in the next section. Then Floquet theory, required to analyze LTP system stability, will be used in section 5.

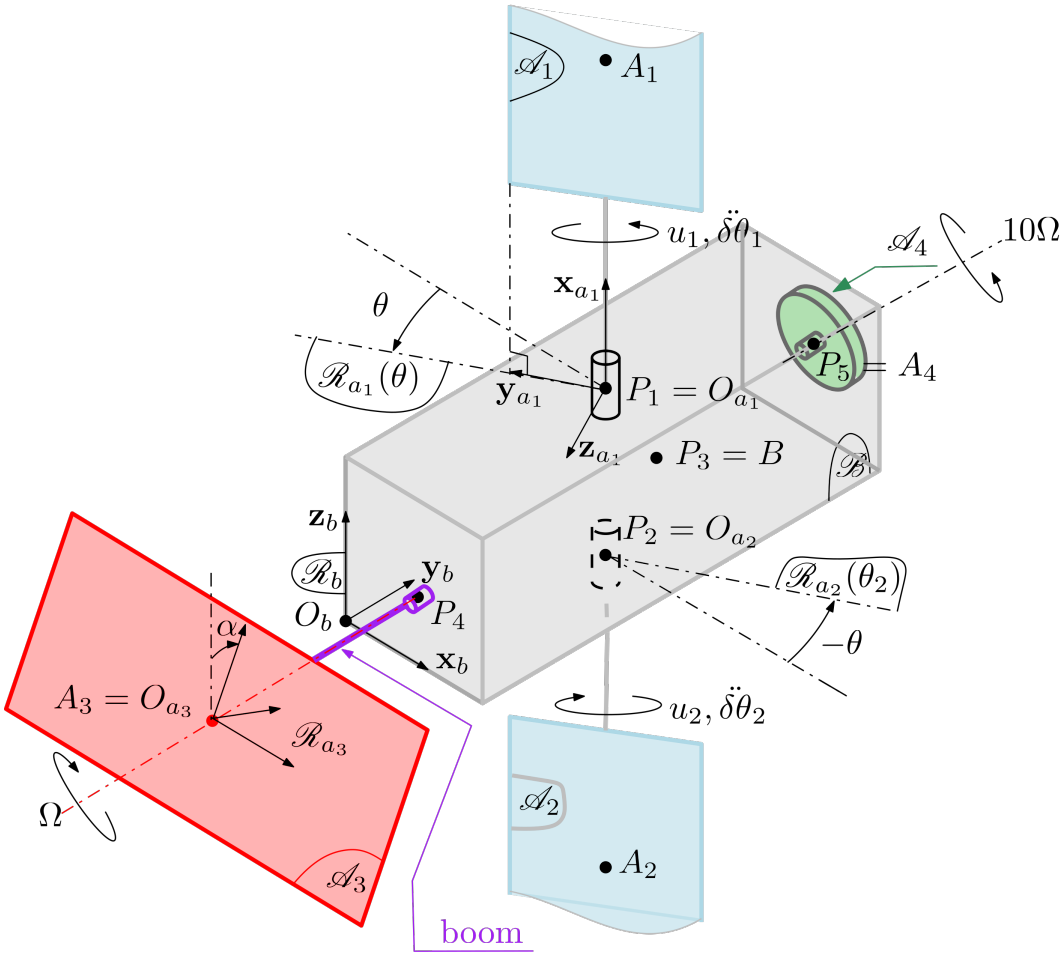

Fig. 9 The study case.

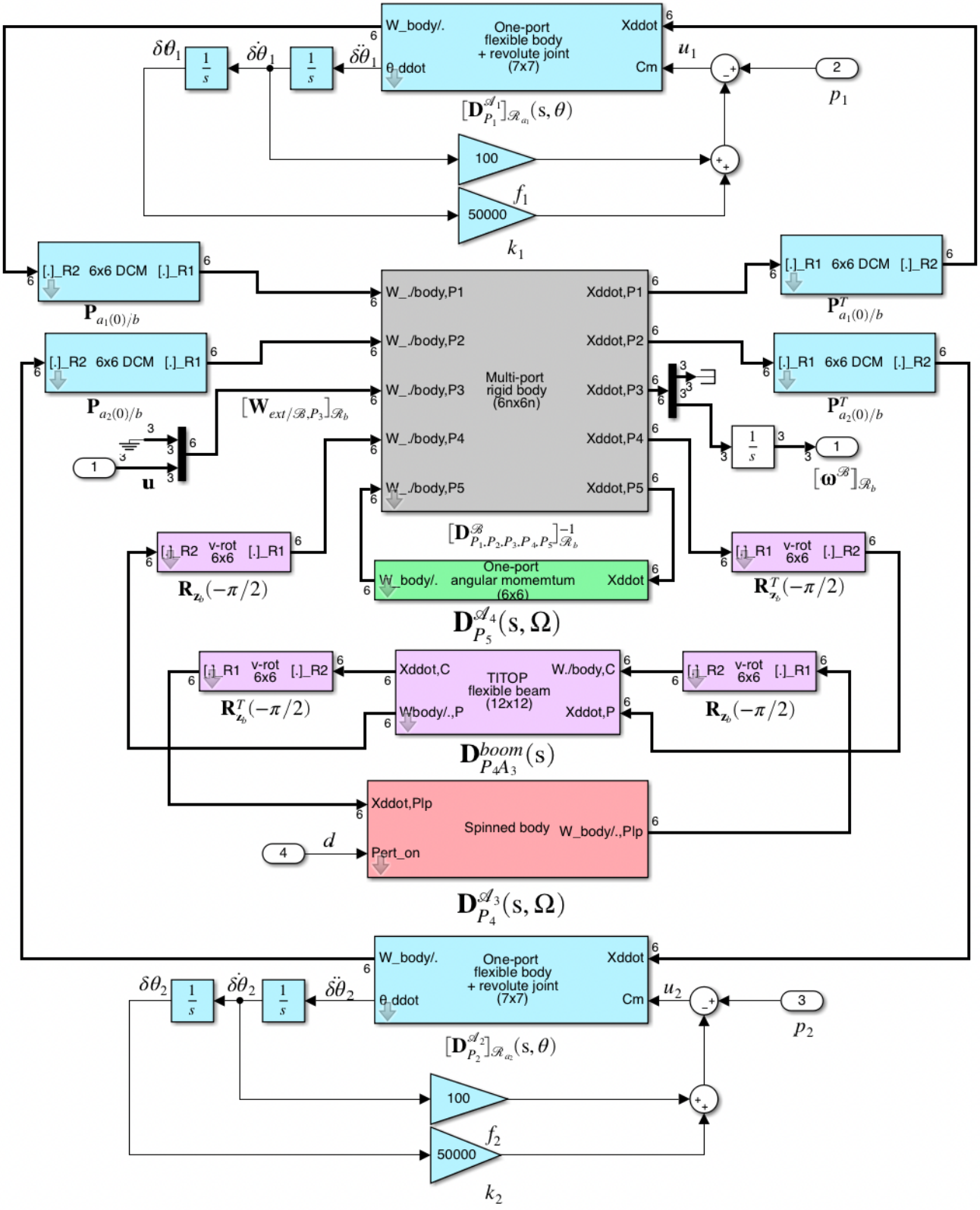

Fig. 10 The SDTlib model $\mathbf{M}(s,\Delta,\theta,\Omega,\Omega t)$ of the study case.

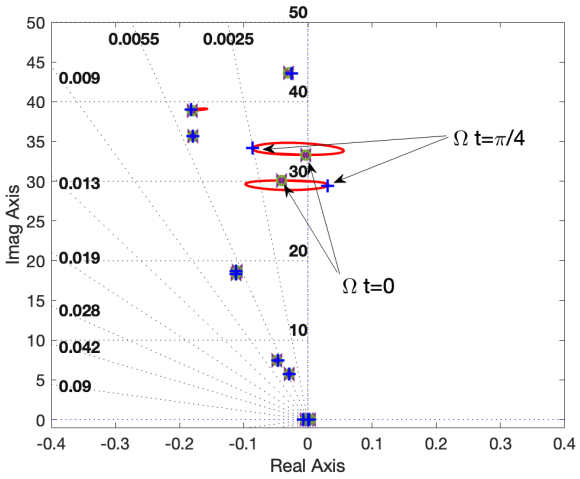

Fig. 11 Evolution of the system dynamics with the RF antenna angular configuration Ωt.

4.2 LTI robust control

The closed-loop model is then described in Figure 12. This model also includes (yellow blocks):

- all the avionics components (`DELAY, RWS, GYRO, SST`) to characterize the dynamics of the reaction wheel system, the gyrometer, the star sensor and the loop delay,
- the weights $[\text{diag}([0.03 \quad 0.01 \quad 0.02])]\,(Nm)$ on the normalized orbital disturbances $\tilde{\mathbf{T}}_{orb}$, $1/\gamma$ on the input sensitivity function and $[\text{diag}([5 \quad 5 \quad 10]\frac{\pi}{18000})]^{-1}\,(rad^{-1})$ on the Absolute Pointing Error (APE). Finally, the filter $F_h(\text{s}, \Omega_c)$ (see Eq. (5)) acts as a weight on the input d_h to account for a harmonic disturbance at the (time-varying) frequency Ω_c, which corresponds to the known actual frequency Ω, even when this closed-loop diagram involves the model $\mathbf{M}(\text{s}, \mathbf{\Delta}, \theta, 0, \Omega t)$ (i.e., with the non-rotating antenna used to perform robust LTI control). Note also that inputs p_1 and p_2 are not weighted because they are not used for the control design and d is already normalized (dimensionless). p_1, p_2 and d will be used in the next section to perform analyzes and robust pointing budgets.

This closed-loop model is thus denoted $\mathbf{P}(\text{s}, \mathbf{\Delta}, \theta, \Omega, \Omega t, \mathbf{K}, \Omega_c)$ to emphasize all the parametric dependencies. The notation $\mathbf{P}(\text{s}, \mathbf{\Delta}, \theta, 0, \Omega t, \mathbf{K}, \Omega)$ indicates that $\Omega = 0$ in the model $\mathbf{M}(\text{s}, \mathbf{\Delta}, \theta, \Omega, \Omega t)$ and that Ω_c is chosen equal to Ω in the control design.

The controller to be optimized is a decentralized control composed, for each of the 3 axes ($i = 1, 2, 3$ for the **x**, **y** and **z**-axis, respectively), of:

- a proportional derivative controller involving the gains K_{p_i} and K_{v_i} ,
- a first order low pass filter involving the frequency λ_i,
- a rejection filter $F_i(\text{s}, \Omega_c)$ centered at the frequency Ω_c and involving 2 additional tuning parameters ξ_{1_i} and d_i.

Thus for each axis, the controller reads:

$$\mathbf{u}_c(i) = -F_i(\text{s}, \Omega)\frac{\lambda_i}{\text{s} + \lambda_i}\left(K_{p_i}\mathbf{\Theta}_m(i) + K_{v_i}\boldsymbol{\omega}_m(i)\right) \quad \text{with:} \quad F_i(\text{s}, \Omega_c) = \frac{d_i\text{s}^2 + 2\xi_{1_i}\Omega_c\text{s} + \Omega_c^2}{\text{s}^2 + 0.002\Omega_c\text{s} + \Omega_c^2}$$

and can be considered as an LPV controller since the frequency Ω_c is a varying parameter.

In the following, $\mathbf{K}$ is the set of the 15 tuning parameters $\mathbf{K} = \{K_{p_i},\ K_{v_i},\ \lambda_i,\ \xi_{1_i},\ d_i,\ \ i = 1, 2, 3\}$.

Three closed-loop transfers will be considered for the robust control design (see Fig. 12):

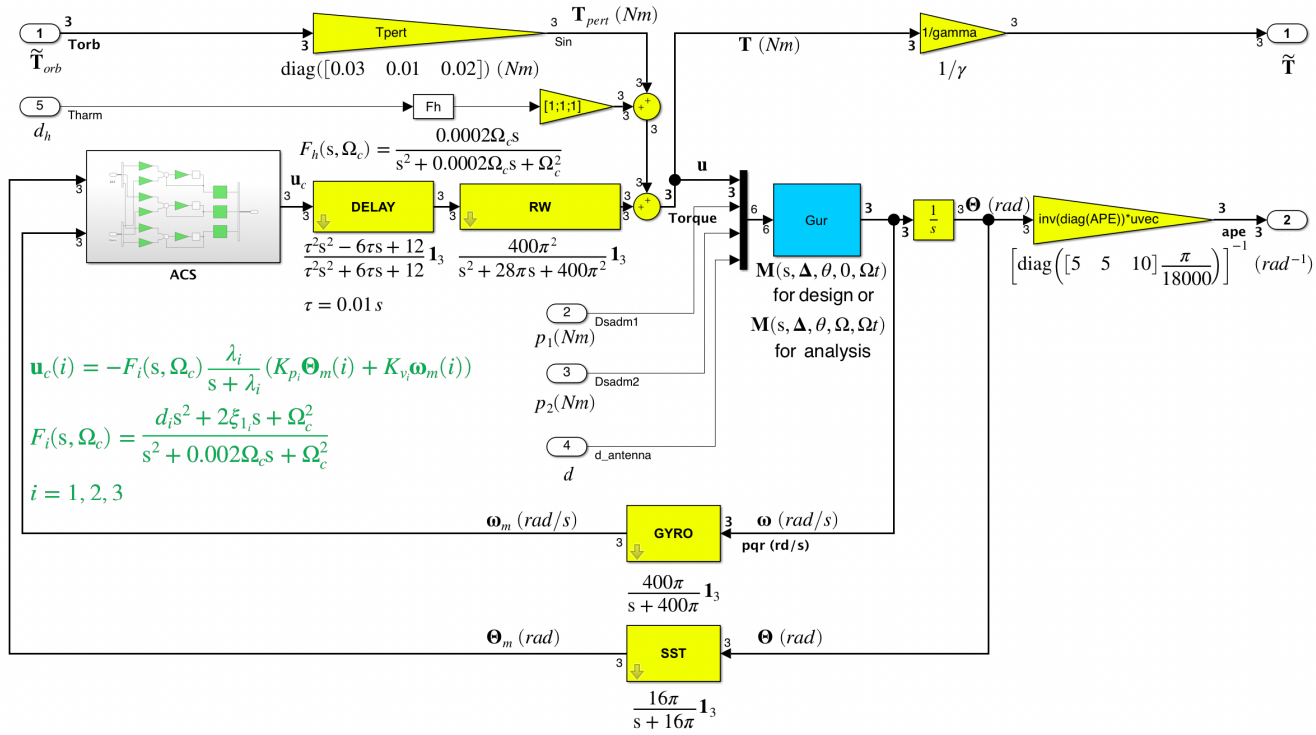

Fig. 12 The closed-loop model $\mathbf{P}(\mathrm{s}, \mathbf{\Delta}, \theta, \Omega, \Omega t, \mathbf{K}, \Omega_c)$.

- $\mathbf{P}_{\tilde{\mathbf{T}}_{orb} \to \tilde{\mathbf{\Theta}}}(\mathrm{s}, \mathbf{\Delta}, \theta, \Omega, \Omega t, \mathbf{K}, \Omega_c)$, from $\tilde{\mathbf{T}}_{orb}$ to $\tilde{\mathbf{\Theta}}$, is the normalized orbital disturbance rejection function on the APE,
- $\mathbf{P}_{d_h \to \tilde{\mathbf{\Theta}}}(\mathrm{s}, \mathbf{\Delta}, \theta, \Omega, \Omega t, \mathbf{K}, \Omega_c)$, from d_h to $\tilde{\mathbf{\Theta}}$ is the harmonic disturbance function on the APE,
- $\bar{\mathbf{S}}(\mathrm{s}, \mathbf{\Delta}, \theta, \Omega, \Omega t, \mathbf{K}, \Omega_c) = \mathbf{P}_{\mathbf{T}_{pert} \to \mathbf{T}}(\mathrm{s}, \mathbf{\Delta}, \theta, \Omega, \Omega t, \mathbf{K}, \Omega_c)$ is the input sensitivity function which can be used to characterize modulus margin.

And the robust control design problem reads:

$$\widehat{\mathbf{K}} = \arg\min_{\mathbf{K}} \max_{\mathbf{\Delta}, \theta, \Omega t, \Omega} \|\mathbf{P}_{d_h \to \tilde{\mathbf{\Theta}}}(\mathrm{s}, \mathbf{\Delta}, \theta, 0, \Omega t, \mathbf{K}, \Omega)\|_\infty = \arg\min_{\mathbf{K}} J(\mathbf{K}) \tag{6}$$

such that:

$$\max_{\mathbf{\Delta}, \theta, \Omega t, \Omega} \|\mathbf{P}_{\tilde{\mathbf{T}}_{orb} \to \tilde{\mathbf{\Theta}}}(\mathrm{s}, \mathbf{\Delta}, \theta, 0, \Omega t, \widehat{\mathbf{K}}, \Omega)\|_\infty \leq 1\,, \tag{7}$$

$$\max_{\mathbf{\Delta}, \theta, \Omega t, \Omega} \|\bar{\mathbf{S}}(\mathrm{s}, \mathbf{\Delta}, \theta, 0, \Omega t, \widehat{\mathbf{K}}, \Omega)\|_\infty \leq \gamma\,. \tag{8}$$

Thus the objective is to minimize the worst-case impact of the harmonic disturbance d_h on the APE while satisfying, on the worst-case parametric configuration, the APE hard requirement in spite of orbital disturbance (eq. (7)) and a second hard requirement on the stability margins (eq. (8)). Indeed the typical value $\gamma = 1.5$ ensures on each of the 3 axes:

- a modulus margin $> 1/\gamma = 0.666$,
- a gain margin $> \frac{\gamma}{\gamma - 1} = 3$ $(6\ dB)$,
- a phase margin $> 2 \arcsin \frac{1}{2\gamma} = 38.9\,(deg)$.

Such a problem can be solved thanks to the interface `slTuner` for control system tuning in Simulink and the Matlab function `systune`. A solution satisfying the 2 hard constraints can be found such that $J(\widehat{\mathbf{K}}) = 0.0306$. The optimal controller gains $\widetilde{\mathbf{K}}$ are given in Table 1.

	i	$K_{p_i}\,(Nm/rad)$	$K_{v_i}\,(Nms/rad)$	$\lambda_i\,(rad/s)$	ξ_{1_i}	d_i
roll	1	34.9	83.0	1.12	−0.252	1.00
pitch	2	11.6	40.7	1.70	−0.725	1.49
yaw	3	11.6	28.8	1.36	−0.335	1.13

Table 1 The optimal controller $\widetilde{\mathbf{K}}$.

A first analysis of this solution is proposed in the next section.

5 LTI and LTP robust performance analysis

In this section the closed-loop system $\mathbf{P}(\mathrm{s}, \boldsymbol{\Delta}, \theta, \Omega, \Omega t, \mathbf{K}, \Omega)$ depicted in Figure 12 is reconsidered with the full model $\mathbf{M}(\mathrm{s}, \boldsymbol{\Delta}, \theta, \Omega, \Omega t)$, thus taking into account the real harmonic disturbance $\left[\overline{\mathbf{W}}_{pert}(\Omega, \Omega t)\right]_{\mathscr{R}_b}$ and the gyroscopic gain $\left[\mathbf{G}_{A_3}^{\mathscr{A}_3}(\Omega, \Omega t)\right]_{\mathscr{R}_b}$, both parametrized according to the varying antenna rate Ω. The objective is to perform robust pointing performance budgets. Thus the frequency-domain responses of the transfers between the various disturbance sources and the normalized APE $\tilde{\boldsymbol{\Theta}}$ are depicted in Figure 13 (top) for 100 randomly sampled parametric configurations. The hard requirement is met when the magnitude is lower than 1 ($0\,dB$). One can conclude from these responses that:

- the orbital disturbances $\widetilde{\mathbf{T}}_{orb}$ (blue lines) saturate the APE requirement (equation (7)) in low frequencies. Note that this is due to the chosen proportional derivative controller structure. An integral action in the controller could improve the performance at very low frequencies. Some "rare" parametric configurations do not meet the requirement around $20 - 30\,rad/s$,
- the harmonic disturbances d due to the antenna dynamic unbalances (red lines) is correctly rejected thanks to the LPV rejection filters $F_i(\mathrm{s}, \Omega)$ for the 3 axes and for any variations of Ω,
- the rejection of the SADMs disturbances p_1 and p_2 (yellow lines) is also satisfactory since a $1\,Nm$ magnitude disturbance (which is quite high) at any frequency is rejected.

Finally, the Figure 13 (bottom) represents the frequency-domain response of the input sensitivity function $\bar{\mathbf{S}}$ which should be lower than the requirement γ (equation (8)). While this requirement is fulfill at low frequencies, some "rare" parametric configurations do not meet the requirement around $20 - 30\,rad/s$.

These violations on the two hard requirements at the frequencies around $20 - 30\,rad/s$ are linked to the LTI nature of the model used for the control design but which is not representative of the real LTP nature of the system. They correspond to the problem depicted in Figure 11 where 2 flexible modes seems instable for some angular configurations of the antenna. But these analyses do not allow to conclude that the stability or the requirements are not met on the LTP model. Indeed, looking for the worst-case gain of the input sensitivity function $\bar{\mathbf{S}}$ (with the MATLAB function `wcgain`) leads to an unstable parametric configuration very close to the nominal one:

$$\boldsymbol{\Delta}_{wc} = [1000.3\,kg \quad 75.\,kgm^2 \quad 40.\,kgm^2 \quad 80.\,kgm^2 \quad 5.586\,rad/s \quad 19.3\,rad/s \quad 35.275\,rad/s]^T,$$

$$\theta_{wc} = 0.8\,deg, \quad \Omega_{wc} = 1.5711\,rad/s, \quad \Omega t_{wc} = 0.8\,deg\,.$$

The frequency of the "unstable" flexible mode is $33.3\,rad/s$. Let us denote $\mathbf{A}_{wc}(\Omega t)$, the time-periodic dynamic matrix of the closed-loop system $\mathbf{P}(\mathrm{s}, \boldsymbol{\Delta}_{wc}, \theta_{wc}, \Omega_{wc}, \Omega t, \widehat{\mathbf{K}})$ evaluated on the worst case configuration except for Ωt which is kept varying. By applying the Floquet theory [12] to analyze the stability of the LTP system, the monodromy matrix $\mathbf{R}_{wc}$ in the worst-case configuration can be approximated by integrating N oversampled LTI systems, evaluated at N regularly spaced instants within a period

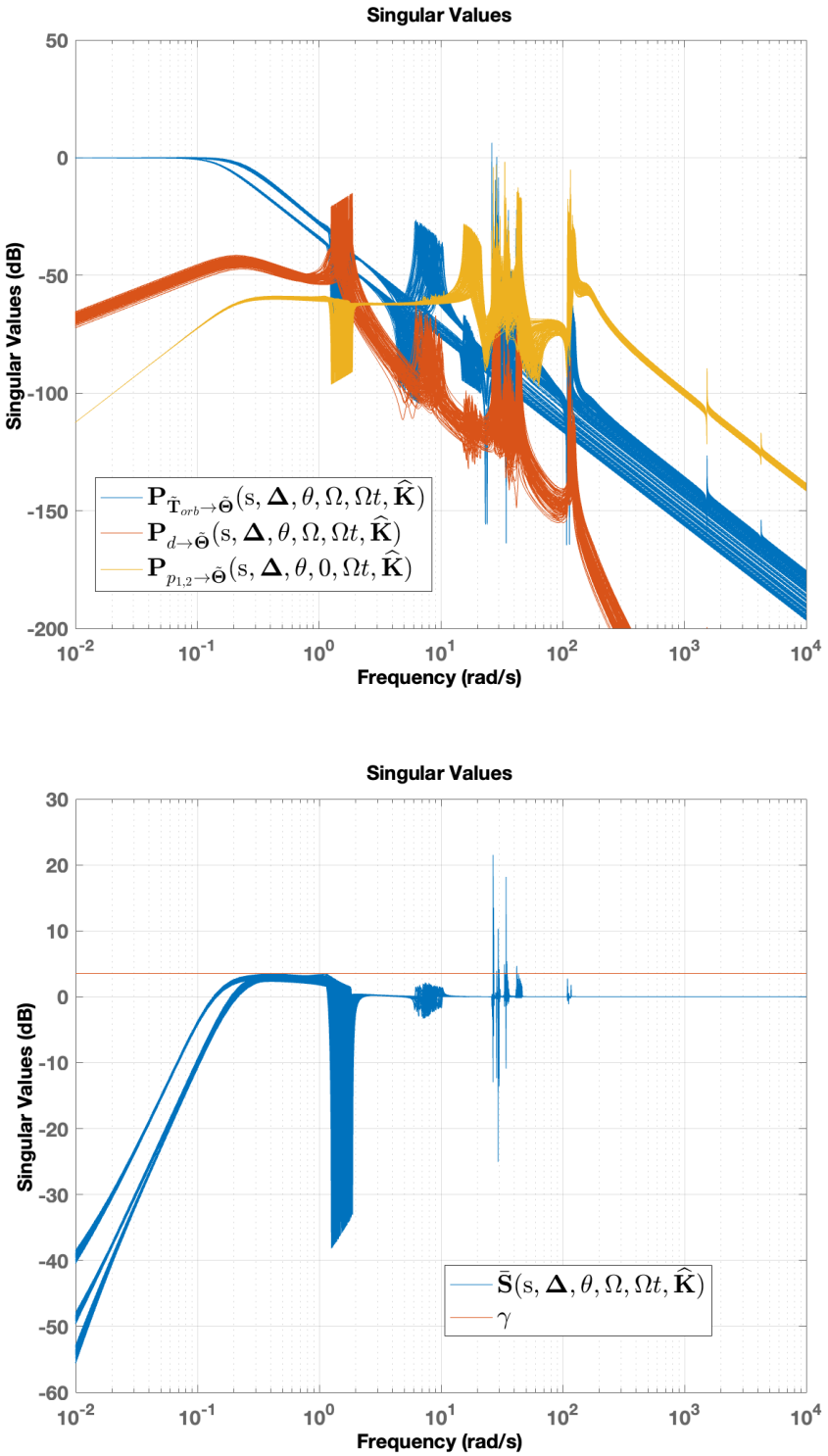

Fig. 13 The frequency-domain responses of the transfers between the various disturbance sources and the normalized APE (top) and the input sensitivity function (bottom) for 100 randomly sampled parametric configurations.

$T = 2\pi/\Omega$:

$$\mathbf{R}_{wc} \approx \Pi_{i=1}^{N-1} e^{\mathbf{A}_{wc}(2\pi i/N)\frac{T}{N}} = e^{\mathbf{A}_{wc}\left(2\pi\frac{N-1}{N}\right)\frac{T}{N}} \cdots e^{\mathbf{A}_{wc}(2\pi/N)\frac{T}{N}} e^{\mathbf{A}_{wc}(0)\frac{T}{N}}.$$

Then it can be easily checked, for instance with $N = 30$, that all the eigenvalues of $\mathbf{R}_{wc}$ have a magnitude lower than 1 and thus that the LTP system $\mathbf{P}(\mathrm{s}, \mathbf{\Lambda}_{wc}, \theta_{wc}, \Omega_{wc}, \Omega t, \widehat{\mathbf{K}})$ is stable. The time-domain responses of the 3 normalized EULER angles $\widetilde{\phi}$, $\widetilde{\theta}$ and $\widetilde{\psi}$ to the harmonic disturbance d are depicted in Figure 14 for this particular worst-case. After a transient response, the response is stable and the APE requirement is met.

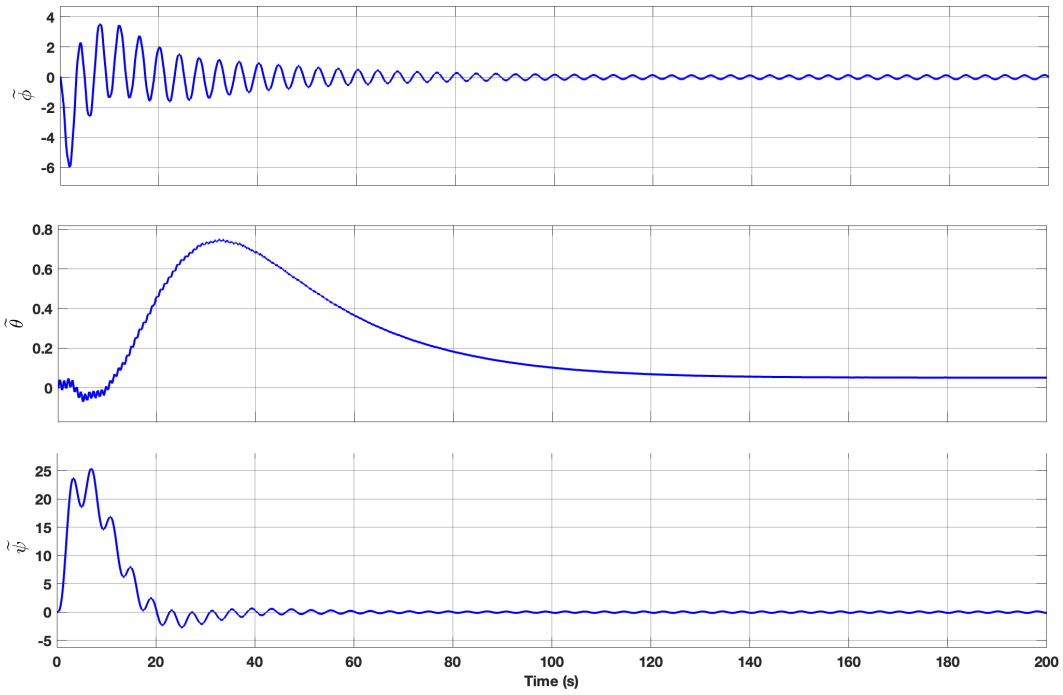

Fig. 14 Time-domain simulation of the spacecraft attitude (normalized APE) in response to the harmonic disturbance d.

These first analyzes make us confident in the proposed control design but a full validation and verification process dedicated to LTP systems is still required.

6 Conclusions

A linear time-periodic model of a rotating antenna was developed under the TITOP formalism, allowing the study of the impact of disturbances caused by dynamic unbalances on the six degrees of freedom of the entire spacecraft, which carries the antenna along with other flexible appendages. A highly structured, decentralized, and robust attitude controller was designed to meet pointing requirements despite harmonic antenna disturbances, orbital perturbations, and internal disturbances in the solar array drive mechanism. This controller employs one linear-parameter-varying rejection filter per axis, adapted to the antenna's angular rate, which is assumed to be known. An initial validation was performed to assess the disturbance rejection performance; however, further analyses are required to fully validate the proposed design, considering the time-periodic nature of the parameter-uncertain system.

Appendix

The data for the proposed study case are presented in Table 2.

Declaration of Use of Artificial Intelligence

Artificial intelligence was not used in the work presented.

References

[1] Cornelius Dennehy and Oscar S. Alvarez-Salazar. Spacecraft Micro-Vibration: A Survey of Problems, Experiences, Potential Solutions, and Some Lessons Learned. Technical Report NASA/TM-2018-220075, NASA, 2018.

[2] Daniel Alazard and Francesco Sanfedino. Satellite dynamics toolbox for preliminary design phase. In *43rd Annual AAS Guidance and Control Conference, 30 January 2020 - 5 February 2020 (Brechenridge, United States)*, pages 1461–1472, 2020.

[3] Daniel Alazard and Francesco Sanfedino. Satellite dynamics toolbox & library. `https://personnel.isae-supaero.fr/daniel-alazard/matlab-packages/satellite-dynamics-toolbox.html`. Accessed: 2020-01-25.

[4] Jawhar Chebbi, Vincent Dubanchet, José Alvaro Perez-Gonzalez, and Daniel Alazard. Linear dynamics of flexible multibody systems: a system-based approach. *Multibody System Dynamics*, 41(1):75–100, 9 2017. ISSN: 1384-5640. doi: 10.1007/s11044-016-9559-y.

[5] Francesco Sanfedino, Daniel Alazard, Valentin Preda, and Davide Oddenino. Integrated modeling of microvibrations induced by solar array drive mechanism for worst-case end-to-end analysis and robust disturbance estimation. *Mechanical Systems and Signal Processing*, 163:108168, 2022. ISSN: 0888-3270. doi: https://doi.org/10.1016/j.ymssp.2021.108168.

[6] Francesco Sanfedino, Gabriel Thiébaud, Daniel Alazard, Nicola Guercio, and Nicolas Deslaef. Advances in fine line-of-sight control for large space flexible structures. *Aerospace Science and Technology*, 130:107961, 2022. ISSN: 1270-9638. doi: https://doi.org/10.1016/j.ast.2022.107961.

[7] Valentin Preda. *Robust microvibration control and worst-case analysis for high pointing stability space missions*. Theses, Université de Bordeaux, Dec. 2017. `https://theses.hal.science/tel-01722860`.

[8] Paolo Iannelli, Federica Angeletti, and Paolo Gasbarri. A model predictive control for attitude stabilization and spin control of a spacecraft with a flexible rotating payload. *Acta Astronautica*, 199:401–411, 2022. ISSN: 0094-5765. doi: https://doi.org/10.1016/j.actaastro.2022.07.024.

[9] S. Bittanti and P. Colaneri. *Periodic Systems: Filtering and Control*. Communications and Control Engineering. Springer London, 2008. ISBN: 9781848009110.

[10] Vincent Dubanchet. *Modeling and control of a flexible space robot to capture a tumbling debris*. PhD thesis, Université de Montréal, 2016.

[11] Wikipedia contributors. Newton–euler equations — Wikipedia, the free encyclopedia, 2025. [Online; accessed 30-September-2025]. `https://en.wikipedia.org/w/index.php?title=Newton%E2%80%93Euler_equations&oldid=1311626019`.

[12] Cevat Gökçek. Stability analysis of periodically switched linear systems using floquet theory. *Mathematical Problems in Engineering*, 2004(1):521989, 2004. doi: https://doi.org/10.1155/S1024123X04401069.

Body	parameter	value	unit
$\mathscr{B}$	$m^{\mathscr{B}}$	$1000 \pm 20\%$	kg
	$\left[\mathbf{I}_B^{\mathscr{B}}\right]_{\mathscr{R}_b}$	$\begin{bmatrix} 75 \pm 20\% & 1 & 2 \\ 1 & 40 \pm 20\% & -1 \\ 2 & -1 & 80 \pm 20\% \end{bmatrix}$	$kg\,m^2$
	$\left[\overrightarrow{O_bP_1}\right]_{\mathscr{R}_b}$	$[0.4 \quad 1.4 \quad 1]^T$	m
	$\left[\overrightarrow{O_bP_2}\right]_{\mathscr{R}_b}$	$[0.4 \quad 1.4 \quad 1]^T$	m
	$\left[\overrightarrow{O_bP_3}\right]_{\mathscr{R}_b}$	$[0.35 \quad 1.5 \quad 0.5]^T$	m
	$\left[\overrightarrow{O_bP_4}\right]_{\mathscr{R}_b}$	$[0.35 \quad 0 \quad 0.5]^T$	m
	$\left[\overrightarrow{O_bP_5}\right]_{\mathscr{R}_b}$	$[0.35 \quad 2 \quad 0.5]^T$	m
$\mathscr{A}_i$, $i = 1, 2$	$m^{\mathscr{A}_i}$	43	kg
	$\left[\mathbf{I}_B^{\mathscr{A}_i}\right]_{\mathscr{R}_{a_i}}$	$\mathrm{diag}[17 \quad 62 \quad 79]$	$kg\,m^2$
	$\left[\overrightarrow{O_{a_i}A_i}\right]_{\mathscr{R}_{a_i}}$	$[2.07 \quad 0 \quad 0]^T$	m
	$\omega_j^{\mathscr{A}_i}$, $j = 1, 2, 3$	$5.6 \pm 20\%$, $19.3 \pm 20\%$, $35.4 \pm 20\%$	rad/s
	$\left[\mathbf{L}_{O_{a_i}}^{\mathscr{A}_i}\right]_{\mathscr{R}_{a_i}}$	$\begin{bmatrix} 0 & 0 & -5.12 & 0 & 12.5 & 0 \\ 0 & 0 & 0 & -2.84 & 0 & 0 \\ 0 & 0 & -2.97 & 0 & 2.51 & 0 \end{bmatrix}$	$\sqrt{kg}$, $\sqrt{kg}m$
	damping ratio	0.005	
	k_i	50000 (SADM local stiffness)	Nm/rad
	d_i	100 (SADM local damping)	Nms/rad
boom	length: $l = \lvert\overrightarrow{P_4O_{a_3}}\rvert$	2.	m
	section: S	0.0025	m^2
	2-nd moment of aera: $I_{y,z}$	$5.2083\,10^{-7}$	m^4
	Young mod.: E	$70\,10^9$	N/m^2
	Poisson coef.: ν	0.35	
	damping ratio	0.001	
$\mathscr{A}_3$	$m^{\mathscr{A}_3}$	20	kg
	$\left[\mathbf{I}_{A_3}^{\mathscr{A}_3}\right]_{\mathscr{R}_{a_3}}$	$\mathrm{diag}[6.683 \quad 13.33 \quad 6.6833]$	$kg\,m^2$
	tilt: α	$\pi/6$	rad
	rate around $\mathbf{y}_b$: Ω	$1.57 \pm 20\%$	rad/s
$\mathscr{A}_4$	$m^{\mathscr{A}_4}$	5.16	kg
	wheel inertia: J_w	$\frac{1}{10}\left[\mathbf{I}_{A_3}^{\mathscr{A}_3}\right]_{\mathscr{R}_b\,2,2}$	$kg\,m^2$
	$\left[\mathbf{I}_B^{\mathscr{A}_4}\right]_{\mathscr{R}_b}$	$\mathrm{diag}[J_w/2 \quad J_w \quad J_w/2]$	$kg\,m^2$
	rate around $\mathbf{y}_b$: -10Ω	$-15.7 \pm 20\%$	rad/s

Table 2 Study-case - list of numerical values and uncertainties.